MINISTRY OF TECHNOLOGY

AERONAUTICAL RESEARCH COUNCIL
REPORTS AND MEMORANDA

Analysis of the Static Pressure Distribution on a Delta Wing in Subsonic Flow

By D. L. I. KIRKPATRICK

Aerodynamics Dept., R.A.E., Farnborough

Analysis of the Static Pressure Distribution on a Delta Wing in Subsonic Flow

By D. L. I. KIRKPATRICK

Aerodynamics Dept., R.A.E., Farnborough

Summary.

The static-pressure distribution on the surface of a thin delta wing of aspect ratio 1·616 was measured at several incidences in subsonic flow, and the results were analysed to investigate the development with incidence of the leading-edge vortices above the wing and of the chordwise distribution of the aerodynamic loading on it. The results were compared with those obtained from ealier tests to demonstrate how the chordwise distribution of aerodynamic loading on a slender wing is affected by its aspect ratio, thickness and wing-tip shape.

LIST OF CONTENTS

---

1. *Introduction.*

In 1946 Jones[1] presented a theory for calculating the aerodynamic normal force on slender wings, but experimental investigations soon showed that this theory was not very accurate. It was found that the flow field above a sharp-edged slender wing at incidence was dominated by vortex sheets springing from the leading edges and rolling up above the wing to form leading-edge vortices which had a considerable effect on the aerodynamic characteristics. A potential-flow theory of the development of such vortices and their effects has been presented by Smith[2] who has shown that the normal-force characteristic of a plane delta wing at incidence α in conical flow is closely approximated by the expression

$$\frac{C_N}{K^2} = 2\pi \left(\frac{\alpha}{K} \right) + 4 \cdot 9 \left(\frac{\alpha}{K} \right)^{1 \cdot 7}, \tag{1}$$

where K is the cotangent of the sweepback angle of the leading edge. The first term on the right hand side of this expression is the linear component of the normal force, which was calculated by Jones[1], and the second term is the non-linear component induced by the leading-edge vortices. The form of this expression has been confirmed by an experimental investigation[3] of the normal forces on conical slender wings of aspect ratio 0·8 in subsonic conical flow; this investigation has shown that

$$\frac{C_N}{K^2} = 2\pi a \left(\frac{\alpha}{K} \right) + b \left(\frac{\alpha}{K} \right)^p, \tag{2}$$

where a, b and p are functions of the shape of the wing's spanwise cross-section and have been determined for wings with various rhombic[3] and biconvex[4] cross-sections.

But studies of the conical flow field provide only the first rung of the ladder towards complete understanding of the complex flow fields round slender wings. These flow fields are generally non-conical because of chordwise variation of the leading-edge sweepback or of the shape of the spanwise cross-section and, in subsonic flow, because of the need to satisfy the Kutta condition at the trailing edge. Thus conical flow studies alone can yield only a qualitative guide to the development with incidence of the flow field round a slender wing in subsonic flow.

Although a considerable quantity of information about the effects of the planform on the aerodynamic forces and moments on a slender wing has been obtained[5] from a series of tests measuring the longitudinal characteristics of various slender wings, there remains the need for more information about the distribution of aerodynamic loading on a slender wing to provide more understanding of the development of the flow field and thus to facilitate the interpretation of the measured characteristics.

2

This Report presents the results of an experiment which was made to measure the static-pressure distribution on a thin delta wing. The measurements were made in sufficient detail to reveal the variation, with incidence and chordwise station, of the spanwise position of the leading-edge vortices and of the value of the minimum static pressure induced below them, and also to permit the analysis of the chordwise variation of the linear and non-linear components of the aerodynamic normal force on the wing. The results of this experiment were compared with those obtained from earlier, less-detailed investigations and demonstrated how the loading distribution on a slender wing depends on its aspect ratio, its thickness and its tip shape.

2. Experimental Equipment and Procedure.

2.1. Description of Wing.

The wing tested had a delta planform with an aspect ratio of 1·616, the leading-edge sweepback angle being 68 degrees. The chordwise cross-sections were all symmetrical and of the same shape, having a maximum thickness/chord ratio of 0·048. The thickness t at a point (x, y) on the surface was given by the expression

$$t(x, y) = \frac{c - x_0}{4} \frac{x - x_0}{c - x_0} \left(1 - \frac{x - x_0}{c - x_0}\right) \left(1 - \tfrac{1}{2} \frac{x - x_0}{c - x_0}\right), \tag{3}$$

where x was the chordwise distance from the apex, y was the spanwise distance from the centreline, $x_0 = y \tan 68°$ and c was the centreline chord of the wing. With this thickness distribution, the local thickness/span ratio $\dfrac{t(x, 0)}{2s}$ decreased smoothly from a limiting value of 0·31 at the apex to zero at the trailing edge, as illustrated in Fig. 1 which shows the planform of the wing and some typical spanwise cross-sections.

Tubes were set into both the upper and lower surfaces of the wing radiating from its apex so that a plane perpendicular to the centreline was intersected by tubes spaced at intervals of 0·10 of the local semispan when $0 \leqslant \left|\dfrac{y}{s}\right| < 0.6$ and at intervals of 0·05 when $0.6 \leqslant \left|\dfrac{y}{s}\right| < 1.0$, as shown in Fig. 2. The tubes were mostly of inside diameter 0·048 in (O.D. = 0·078 in) but near the apex where space was restricted smaller tubes of inside diameter 0·020 in (O.D. 0·048 in) were used. Holes, of diameter 0·95 mm and 0·45 mm respectively, were drilled in the larger and smaller tubes in spanwise rows 0·05 of the root chord apart on both surfaces of the wing. Each row consisted of 54 holes except for the two rows closest to the apex where lack of space precluded the presence of all the tubes, and the rows were intersected by the cleats or the trailing edge sting and had a slightly smaller number of holes in consequence.

2.2. Experimental Procedure.

The wing, with all its pressure holes sealed with tape, was hung on a standard wire rig in the R.A.E. No. 1 $11\tfrac{1}{2}$ ft $\times$ $8\tfrac{1}{2}$ ft wind-tunnel. Lengths of plastic tubing were attached to the protruding tips of the tubes set in the wing and connected to a sloping multi-tube 40 inch manometer. Each of the spanwise rows of holes was then unsealed in turn and the static-pressure distribution along the unsealed row of holes was measured and recorded at incidences spaced at 2 degree intervals between -2 and 26 degrees. All the tests were made at a wind speed of 120 ft/sec corresponding to a Reynolds number, based on the wing's centreline chord, of 3·15 million; no attempt was made to influence the transition of the boundary layer on the wing.

3. Calculation and Discussion of Results.

3.1. Calculation of Results.

The films containing the photographs of the static-pressure distributions along each row of holes at each incidence were put on to a Benson-Lehner 'Boscar' film reader and the value of the static pressure at

each hole was read from the film and punched on to a data card. These cards were then fed into an automatic graph plotter, which produced graphs of the spanwise static-pressure distribution at each angle of incidence at each chordwise station. A typical graph, with a sketch of the associated flow field, is shown in Fig. 3. From each of these graphs were obtained the minimum values of the static pressure on each side of the wing and the spanwise positions of these minima; the area enclosed by each graph was then measured using a planimeter to find the local normal-force coefficient

$$C_N(x) = \tfrac{1}{2} \int\limits_{-1}^{1} \Delta C_P \, d\left(\frac{y}{s}\right), \tag{4}$$

where y is measured perpendicular to the wing's centreline and s is the local semi-span. The values of the local normal-force coefficient measured where x/c was 0·60 were then corrected for the local effect of the presence of the cleats by adding a small increment ΔC_N such that at zero incidence $C_N(x)$ was zero, and the values measured where x/c was 0·90 and 0·95 were similarly corrected for the effect of the protruding tips of the tubes set into the wing. The results were also corrected for the effects of wind-tunnel blockage and constraint by the methods given by Pankhurst and Holder [6] and Berndt [7] respectively.

The spanwise pressure distributions showed slight differences between the pressures measured at the same distance from the centreline on the port and starboard sides of the wing, indicating that the angle of yaw was not exactly zero due to a slight non-uniformity in the wind-tunnel flow. Since the principal purpose of this experiment was to determine the chordwise variation of the local normal-force coefficient $C_N(x)$ and since this coefficient has been shown[8,9] to be unaffected by small angles of yaw, no yaw correction has been applied to the results. The effect of the yaw angle on the measured pressure distributions was small but distinct so the values and spanwise positions of the static pressure minima on different sides of the wing were plotted separately.

3.2. Strength and Position of the Leading-Edge Vortices.

The largest negative values of the static-pressure coefficient on the port and starboard sides of the pressure-distribution curves at each chordwise station were plotted in Fig. 4. The two parts of this figure both show that as x/c increased from zero at the apex the modulus of the minimum static-pressure coefficient rose, attaining its largest value when $\frac{x}{c} \simeq \tfrac{1}{4}$, and that as x/c tended to 1·0 at the trailing edge the modulus decreased towards zero. It has been shown[3] that the aerodynamic normal force induced by the leading-edge vortices on a wing in conical flow is dependent on the thickness/span ratio and increases as this ratio decreases, so it is reasonable to assume that the increase of $\left|C_{P_m}\right|$, as x/c increased from zero, is associated with the concurrent decrease of the thickness/span ratio. The decrease of $\left|C_{P_m}\right|$ as x/c tended to 1·0 shows the effect on the flow field of the need to satisfy the Kutta condition at the trailing edge; the importance of this effect is emphasized by the fact that at large incidence the value of $\left|C_{P_m}\right|$ at $\frac{x}{c} = 0.95$ is only a fifth of its value near the apex. Fig. 4 also shows that as the incidence was increased beyond 20 degrees the hitherto smooth increase of $\left|C_{P_m}\right|$ with incidence ceased near the trailing edge, especially on the port side where $\left|C_{P_m}\right|$ for $0.5 < \frac{x}{c} < 1.0$ decreased as the incidence was increased from 20 to 25 degrees. This decrease is consistent with the occurrence above this part of the wing of the phenomenon known as vortex breakdown which is discussed in Section 3.3 and in the Appendix.

The spanwise positions of the static-pressure minima are plotted in Fig. 5 which, like Fig. 4, show slight differences between the values measured on different sides of the wing. Fig. 5 shows that as t incidence was increased the leading-edge vortices moved inboard, as illustrated by the Table below.

4

Chordwise station, $\dfrac{x}{c}$	0·25					
Angle of incidence, α	0	5	10	15	20	25
Spanwise position of minimum, $\dfrac{y_m}{s}$	1·0	0·88	0·80	0·74	0·71	0·70

The effect of the presence of the trailing edge made the vortices more inboard as they approached it, i.e. y_m/s decreased as x/c tended to 1·0, in a manner similar to that observed by Peckham[10].

Angle of incidence, α	25								
Chordwise station, $\dfrac{x}{c}$	0·1	0·2	0·3	0·4	0·5	0·6	0·7	0·8	0·9
Spanwise position of minimum, $\dfrac{y_m}{s}$	0·65	0·70	0·70	0·70	0·69	0·69	0·68	0·67	0·65

This Table, and both parts of Fig. 5, show that the spanwise position of C_{P_m} varied between the chordwise stations $\dfrac{x}{c} = 0\cdot 1$ and $\dfrac{x}{c} = 0\cdot 2$. The spanwise pressure distributions at these stations show that this change was associated with a decrease in the effect of the secondary vortex, this decrease being due to boundary-layer transition between these two stations. The change in y_m/s due to transition was similar in magnitude and direction to that previously measured by Earnshaw[11].

3.3. Distribution of the Local Normal-Force Coefficient $C_N(x)$.

The local values of the normal-force coefficient $C_N(x)$ obtained at each incidence at each chordwise station (see Table 1) are plotted in Fig. 6 which shows how $C_N(x)$ decreased towards zero at the trailing edge. Since the thickness/span ratio of the wing was nowhere large and since ds/dx was not a function of x/c, the flow field round the wing would have been nearly conical if there had been no trailing-edge effect, and $C_N(x)$ would have been almost independent of x/c. However Fig. 6 shows that at low incidences there was an appreciable trailing-edge effect on the value of $C_N(x)$ where $0\cdot 5 < \dfrac{x}{c} \leqslant 1$ and that at higher incidences the values of $C_N(x)$ at all chordwise stations were affected.

The values of $C_N(x)$ obtained at several incidences were multiplied by the appropriate value of $\dfrac{s}{b/2}$, where b is the wing span, to obtain the chordwise distributions of aerodynamic loading (see Table 2) which were then plotted in Fig. 7. This figure shows that as the incidence was increased the wing's centre of pressure, whose chordwise position is given by the equation

$$\left(\frac{x}{c}\right)_{\text{c.p.}} = \frac{\displaystyle\int_0^c \frac{x}{c}\,\frac{s}{b/2}\,C_N(x)\,dx}{\displaystyle\int_0^c \frac{s}{b/2}\,C_N(x)\,dx}, \tag{5}$$

moved forward, thus decreasing the static longitudinal stability of the wing. This forward movement of the centre of pressure with increasing incidence is a characteristic feature of slender wings and has been

5

observed and discussed by several investigators, notably Peckham[10] and Kirby[5]. The areas under the aerodynamic loading curves were then measured with a planimeter to find the values of the normal-force coefficient on the wing from the equation

$$C_N = 2 \int_0^1 \frac{s}{b/2} C_N(x) \, d\left(\frac{x}{c}\right).$$

(6)

The values of C_N were plotted in Fig. 8 along with the normal-force characteristic measured[12] on a wind-tunnel balance. This figure shows that above an incidence of 20 degrees the C_N values obtained by integrating the static-pressure distribution differed from those obtained from balance measurements. The difference suggests that breakdown of at least one of the leading-edge vortices occurred above the wing, during the pressure measurements but not during the balance measurements, when the incidence exceeded 20 degrees. The results of an experimental investigation of vortex breakdown by Earnshaw[13] indicated that it would not occur above this delta wing at incidences below 27 degrees; this forecast was supported by the balance measurements[12] which showed no effects of vortex breakdown below an incidence of 25 degrees. However it appears that, during the tests to measure the static-pressure distribution, breakdown of a leading-edge vortex above the wing occurred at a lower incidence, probably because of the presence of the bundle of plastic tubing downstream of the trailing edge, for it is well-known that vortex breakdown is particularly sensitive to the presence of obstructions in the flow[14,15]. To avoid confusion, the analysis in Section 4 below concerning the trailing-edge effect and the thickness effect on the chordwise distribution of $C_N(x)$ includes only values measured at incidences below 20 degrees; the effects of vortex breakdown are discussed separately in the Appendix.

4. *Analysis of Results.*

4.1. *The Linear Component of the Normal Force.*

The results of this experiment were analysed by separating the measured normal-force coefficients at each chordwise station into their linear and non-linear components, as suggested by Smith's theory[2] (*see* Section 1). The linear component of the local normal force is defined as $\alpha \left(\dfrac{\partial C_N(x)}{\partial \alpha}\right)_0$, where $\left(\dfrac{\partial C_N(x)}{\partial \alpha}\right)_0$ is the slope of the local normal-force characteristic at zero incidence. Although it was not possible to determine this slope accurately from the measured pressure distributions, it was feasible to obtain an approximate value of the slope at each chordwise station from the expression

$$\left(\frac{\partial C_N(x)}{\partial \alpha}\right)_0 = \frac{180}{4\pi} \left[C_N(x)_{+2} - C_N(x)_{-2}\right],$$

(7)

where $C_N(x)_{+2}$ and $C_N(x)_{-2}$ were the values of $C_N(x)$ measured at incidences of $+2$ and -2 degrees respectively, and these values are plotted in Fig. 9a. Using these results it was calculated that at zero incidence the slope of the wing's normal-force characteristic was

$$\frac{\partial C_N}{\partial \alpha} = 2 \int_0^1 \frac{s}{b/2} \left(\frac{\partial C_N(x)}{\partial \alpha}\right)_0 d\left(\frac{x}{c}\right) = 1 \cdot 72$$

(8)

and the chordwise position of its centre of pressure was

6

$$\left(\frac{x}{c}\right)_{c.p.} = \frac{2}{1\cdot72} \int_0^1 \frac{s}{b/2}\left(\frac{\partial C_N(x)}{\partial \alpha}\right)_0 \frac{x}{c}\, d\left(\frac{x}{c}\right) = 0\cdot597 . \tag{9}$$

These values are sufficiently close to those obtained from balance measurements[12] to prove that the curve in Fig. 9a is a close approximation to the true distribution of $\left(\dfrac{\partial C_N(x)}{\partial \alpha}\right)_0$ and can reasonably be used in the analysis below.

Slender-body theory, which neglects the effects of viscosity and of the presence of the trailing edge, predicts that the linear component of the normal force on a symmetrical slender wing forward of the chordwise station x from the apex is

$$\overline{N}_l = 2\pi\alpha\, q\, s^2\, a(x), \tag{10}$$

where $a(x)$ is a function of the shape of the spanwise cross-section. This force may be non-dimensionalized to obtain the coefficient

$$\overline{C}_{N_l} = \overline{N}_l/4qs^2 = \frac{\pi}{2}\alpha\, a(x). \tag{11}$$

An experimental value of the linear component can be obtained from the test results using the expression

$$\overline{N}_l = q\alpha \int_0^x \left(\frac{\partial C_N(x')}{\partial \alpha}\right)_0 2s(x')\, dx' . \tag{12}$$

Therefore
$$\overline{C}_{N_l} = \frac{\alpha}{4}\frac{cb}{s^2(x)} \int_0^{x/c} \left(\frac{\partial C_N(x')}{\partial \alpha}\right)_0 \frac{s(x')}{b/2}\, d\left(\frac{x'}{c}\right). \tag{13}$$

The chordwise distributions of the theoretical and experimental values of $\overline{C}_{N_l}/\alpha$ (*see* Table 3) are plotted in Fig. 9b, which shows that near the apex the experimental value was slightly less than the theoretical, probably due to the effect of viscosity, but that as x/c increased towards unity the experimental value diverged from the theoretical due to the need to satisfy the Kutta condition of zero loading at the trailing edge in subsonic flow. Thus the linear component of the normal force on the wing was reduced to about two-thirds of the value predicted by slender-body theory.

4.2. *The Non-Linear Component of the Normal Force.*

The chordwise distribution of the parameter $C_N(x)/\alpha$ at three incidences (*see* Table 4) are plotted in Fig. 10a which shows the relative size of the linear and non-linear components of the local normal force.

$$\text{Linear component} \quad = \alpha\left(\frac{C_N(x)}{\alpha}\right)_0$$

$$\text{Non-linear component} = \alpha\left\{\frac{C_N(x)}{\alpha} - \left(\frac{C_N(x)}{\alpha}\right)_0\right\}.$$

This figure shows that the non-linear component is largest near the apex.

7

The chordwise distributions, at two chosen incidences, of the non-linear component of the normal force on the wing forward of the chordwise station x from the apex were calculated using the expression

$$\bar{C}_{N_{nl}} = \frac{\alpha}{4}\frac{cb}{s^2}\int_0^{x/c} \frac{s(x')}{b/2}\left\{\frac{C_N(x')}{\alpha} - \left(\frac{C_N(x')}{\alpha}\right)_0\right\}d\left(\frac{x'}{c}\right) \tag{14}$$

and plotted in Fig. 10b. No theory for predicting such a distribution has yet been presented, but it is interesting to compare the experimental values on $\bar{C}_{N_{nl}}$ at the trailing edge with values calculated using Smith's theory[2] for a plane delta wing of the same aspect ratio in conical flow.

x/c	1·0	1·0
α degree	8	16
$\bar{C}_{N_{nl}}/\alpha$ (expt)	0·23	0·43
$\bar{C}_{N_{nl}}/\alpha$ (theory)	0·61	0·96

This Table shows that the combined effects of the wing's thickness and the presence of its trailing edge reduce the non-linear component to less than half of the theoretical value.

4.3. *Comparison of the Loading Distribution with those on other Delta Wings.*

Smith's theory[2] for calculating the normal force on plane delta wings in conical flow predicts that at a given value of α/K the parameter $C_N(x)/K^2$ is independent of aspect ratio. It is therefore useful to plot the chordwise distributions of the aerodynamic-loading parameter $\dfrac{s}{b/2}\dfrac{C_N(x)}{K^2}$ (*see* Table 5) for delta wings of different thickness and aspect ratio to demonstrate how the loading distribution on a wing is affected by its thickness and its aspect ratio.

Figs. 11a and 11b show the chordwise distributions of the aerodynamic-loading parameter, at a chosen value of α/K, obtained from the results of tests on several delta wings[10,16,17,18]. While differences between the wing designs (e.g. different thickness distributions) preclude a detailed comparison of these loading distributions, two principal effects are apparent, *viz.*

(i) as the aspect ratio of a delta wing increases, the effect of the presence of the trailing edge increases in magnitude at any chordwise station and extends further forward, as shown in Fig. 11a, and

(ii) as the thickness of a delta wing increases (with a concurrent increase of the local thickness/span ratio, especially near the apex), the aerodynamic loading near the apex is significantly reduced, as forecast by slender-body theory and by experimental results[3] for wings in conical flow. Thus the static longitudinal stability of a slender wing may be altered by changing its thickness or its thickness distribution.

4.4. *Comparison of the Chordwise Loading Distributions on a Delta and a Mild Gothic Wing.*

The chordwise loading distributions measured on the delta wing at incidences of 8 and 16 degrees were compared with those obtained from earlier tests on a mild gothic wing[19] (*see* Table 6). The thickness distribution of this mild gothic wing was identical with that of the delta wing (*see* Section 2.1), but the local semispan was given by the equation

$$\frac{s}{b/2} = 1\cdot1\frac{x}{c} - 0\cdot1\left(\frac{x}{c}\right)^{11} \tag{15}$$

and the principal dimensions were as tabulated below

Wing	c in	b in	Area sq in	A	Max $\dfrac{t}{c}$	$\dfrac{ds}{dx}$
Mild gothic	50	36·73	995·6	1·36	0·048	$0\cdot404\left(1-\left(\dfrac{x}{c}\right)^{10}\right)$
Delta	50	40·40	1010	1·616	0·048	0·404

Fig. 12 shows the chordwise variation of the local normal-force coefficient $C_N(x)$ and the normal-force coefficient $\bar{C}_N$ for both wings. When studying this figure, it is appropriate to remember the predictions of slender-body theory that

$$C_N(x) = \pi\alpha\left(2a\frac{ds}{dx}+s\frac{da}{dx}\right) \tag{16}$$

and

$$\bar{C}_N = \frac{\pi}{2}\alpha a \tag{17}$$

for, although this theory takes no account of the presence of the trailing-edge or of the leading-edge vortices, it is nevertheless useful as a basis for comparing different wings. Fig. 12 shows that for $0 < \dfrac{x}{c} < 0\cdot6$, where the two wings are virtually identical, the local normal-force coefficient on the mild gothic wing is slightly greater than that on the delta, indicating that the trailing-edge effect on a slender wing of delta planform extends farther forward than that on a wing with streamwise tips. Fig. 12 also shows that the chordwise distribution of $\bar{C}_N$ for the mild gothic wing with streamwise tips is closer to the distribution predicted by slender-wing theory, i.e. $\bar{C}_N$ for thin wings is almost independent of x/c, than the $\bar{C}_N$ distribution for the delta wing. It is evident that a slight alteration of the tip shape of a slender wing has a significant effect on the flow field round the wing and hence on its longitudinal characteristics (*see* Table 7 and Fig. 13).

5. *Concluding Remarks.*

The results of this experiment showed how the spanwise position of the leading-edge vortices, the static-pressure coefficient below them, and the local aerodynamic normal-force coefficient varied with incidence at 18 chordwise stations along a slender delta wing. As the incidence was increased the vortices above each station moved inboard and the modulus of the minimum static-pressure coefficient below each vortex increased. As the chordwise coordinate x increased from zero at the apex, the modulus of the minimum static-pressure coefficient at a given incidence increased, due to the concurrent decrease of the wing's local thickness/span ratio, to a maximum value about $x = \dfrac{c}{4}$ and then decreased towards zero at the trailing edge because of the need to satisfy the Kutta condition there. The spanwise position of the vortices above the rear of the wing was also affected by the presence of the trailing edge and moved inboard as x/c approached unity.

Analysis of the chordwise distribution of aerodynamic loading showed that both the linear and non-linear components of the local normal-force coefficient were affected by the presence of the trailing edge, but that the effect on the non-linear component, i.e. the component induced by the leading-edge vortices,

is more severe. Consequently, as the wing's incidence was increased and the non-linear component became larger relative to the linear, the centre of pressure moved forward decreasing the wing's static stability.

Comparison of the loading distribution on this wing with those measured on other wings demonstrated how the loading distribution on a slender wing is affected by its aspect ratio, its thickness and the shape of its wing tips.

———— ————

LIST OF SYMBOLS

a	Linear normal-force parameter
A	Aspect ratio
b	Span; non-linear normal-force parameter
c	Centreline chord
C_D	Drag coefficient
C_L	Lift coefficient
C_M	Pitching-moment coefficient, measured about $\dfrac{x}{c} = 0.57$
C_N	Normal-force coefficient
$C_N(x)$	Local normal-force coefficient
$\bar{C}_N$	$\bar{N}/4qs^2$
C_p	Static-pressure coefficient
K	Cotangent of the leading-edge sweepback angle
N	Normal force on the wing
$\bar{N}$	Normal force on the wing forward of a given chordwise station
p	Non-linear normal-force parameter
q	Dynamic pressure
s	Local semi-span
t	Thickness
x	Chordwise distance from apex
y	Spanwise distance from centreline
α	Angle of incidence, in radians unless otherwise stated

Subscripts

c.p.	Measured at the centre of pressure
l	Linear component
m	Measured at a static-pressure minimum
nl	Non-linear component
o	Measured at zero incidence

11

REFERENCES

No.	Author(s)	Title, etc.

1   Robert T. Jones   ..   ..   Properties of low aspect ratio pointed wings at speeds below and above the speed of sound.
NACA T.N. 1032 (A.R.C. 9483) (1946).

2   J. H. B. Smith ..   ..   ..   Improved calculations of leading-edge separation from slender delta wings.
R.A.E. Technical Report 66070 (1966).

3   D. L. I. Kirkpatrick   ..   ..   Investigation of the normal force characteristics of slender delta wings with various rhombic cross-sections in subsonic conical flow.
A.R.C. C.P. 922 (1965).

4   D. L. I. Kirkpatrick   ..   ..   Unpublished.

5   D. A. Kirby   ..   ..   ..   An experimental investigation of the effect of planform shape on the subsonic longitudinal stability characteristics of slender wings.
A.R.C. R. & M. 3568 (1967).

6   R. C. Pankhurst and ..   ..   *Wind-tunnel technique*, chapter 8. Pitman, London (1948).
D. W. Holder

7   Sune B. Berndt   ..   ..   Wind-tunnel interference due to lift for delta wings of small aspect ratio.
KTH Aero. T.N. 19, September 1950.

8   J. K. Harvey   ..   ..   ..   Some measurements on a yawed slender delta wing with leading-edge separation.
A.R.C. R. & M. No. 3160 (1958).

9   D. Hummel   ..   ..   ..   Untersuchung über das Aufplatzen der Wirbel an schlanken Deltaflügeln.
Z. Flugwiss. Heft 5 (1965).

10   D. H. Peckham   ..   ..   Low-speed wind-tunnel tests on a series of uncambered slender pointed wings with sharp edges.
A.R.C. R. & M. 3186 (1958).

11   P. B. Earnshaw   ..   ..   Unpublished.

12   D. L. I. Kirkpatrick   ..   ..   Experimental investigation of the ground effect on the subsonic longitudinal characteristics of a delta wing of aspect ratio 1·616.
R.A.E. Technical Report 66179 (1966). A.R.C. 28407.

13   P. B. Earnshaw   ..   ..   Measurement of vortex breakdown position at low speed on a series of sharp edged symmetrical models.
A.R.C. C.P. 828 (1964).

REFERENCES—*continued*

No.	*Author(s)*	*Title, etc.*

14 D. L. I. Kirkpatrick .. .. Experimental investigation of the breakdown of a vortex in a tube.
A.R.C. C.P. 821 (1964).

15 R. F. A. Keating .. .. Unpublished.

16 D. A. Lemaire .. .. .. Some observations of the low speed flow over a sharp-edged delta wing of unit aspect ratio.
ARL/A Report 126.

17 D. Hummel .. .. .. Private communication.

18 D. J. Marsden, ... The flow over delta wings at low speeds with leading-edge separation.
R. W. Simpson and
W. J. Rainbird C.O.A. Report No. 114 (A.R.C. 20409) (1957).

19 D. J. Kettle .. .. .. Unpublished.

13

APPENDIX

Effects of Vortex Breakdown.

In order to investigate more closely the effects of the breakdown of the leading-edge vortices on the local value of $C_N(x)$, the static-pressure distributions at the chordwise stations where $0 \cdot 7 \leqslant \dfrac{x}{c} \leqslant 0 \cdot 95$ were measured at incidences spaced one degree apart between 20 and 26 degrees. The areas enclosed by the pressure distributions on the port and starboard sides of the wing were measured separately with a planimeter to obtain

$$C_N(x) = \int_{-1}^{0} \Delta C_P \, d\left(\frac{y}{s}\right) \quad \text{[port]}$$

and

$$C_N(x) = \int_{0}^{+1} \Delta C_P \, d\left(\frac{y}{s}\right) \quad \text{[starboard]}$$

and these values are plotted in Fig. 14. This figure shows that, at any chordwise station on either side of the wing, the value of $C_N(x)$ rose as the wing incidence was increased up to the incidence where vortex breakdown was about to occur above that station. Further increase of incidence then caused a sharp drop in $C_N(x)$, followed by another rise. Fig. 14 suggests that the drop in the value of $C_N(x)$ when breakdown occurred was approximately equal to one-tenth of the value just before breakdown. The asymmetry in the chordwise variation with incidence of vortex breakdown on the two sides of the wing was probably due to its small angle of yaw, as shown by Peckham[10], and to asymmetry in the arrangement of plastic tubes behind it (*see* Section 3.3).

TABLE 1

Variation with Incidence and Chordwise Station of the Local Normal-Force Coefficient.

$$C_N(x) = \tfrac{1}{2} \int_{-1}^{1} \Delta C_P \, d\left(\frac{y}{s}\right)$$

$\dfrac{x}{c}$	Angle of incidence, degree					
	4	8	12	16	20	24
0·10	0·175	0·415	0·715	1·080	1·525	2·015
0·15	0·180	0·420	0·725	1·080	1·505	1·955
0·20	0·185	0·425	0·725	1·075	1·460	1·880
0·25	0·185	0·425	0·720	1·045	1·405	1·800
0·30	0·185	0·415	0·700	1·025	1·385	1·760
0·35	0·180	0·405	0·675	1·000	1·330	1·670
0·40	0·185	0·410	0·670	0·975	1·290	1·600
0·45	0·175	0·390	0·650	0·940	1·235	1·525
0·50	0·170	0·380	0·635	0·905	1·175	1·425
0·55	0·170	0·370	0·610	0·865	1·130	1·330
0·60	0·155	0·350	0·575	0·815	1·065	1·245
0·65	0·140	0·325	0·535	0·765	1·010	1·160
0·70	0·135	0·310	0·510	0·725	0·945	1·070
0·75	0·135	0·300	0·475	0·665	0·850	0·970
0·80	0·125	0·270	0·435	0·605	0·775	0·880
0·85	0·110	0·240	0·380	0·525	0·650	0·750
0·90	0·100	0·205	0·305	0·405	0·510	0·595
0·95	0·070	0·130	0·195	0·260	0·325	0·395

TABLE 2

Variation with Influence and Chordwise Station of the Local Loading Coefficient

$$\frac{s}{b/2} C_N(x)$$

$\dfrac{x}{c}$	Angle of incidence, degree					
	4	8	12	16	20	24
0·10	0·017	0·042	0·072	0·108	0·153	0·201
0·15	0·027	0·063	0·107	0·162	0·226	0·294
0·20	0·037	0·085	0·145	0·215	0·292	0·376
0·25	0·046	0·106	0·180	0·261	0·351	0·450
0·30	0·055	0·124	0·210	0·307	0·415	0·528
0·35	0·063	0·142	0·236	0·350	0·465	0·584
0·40	0·074	0·164	0·268	0·390	0·516	0·640
0·45	0·079	0·175	0·292	0·423	0·505	0·686
0·50	0·085	0·190	0·317	0·452	0·587	0·712
0·55	0·093	0·203	0·335	0·476	0·621	0·731
0·60	0·093	0·210	0·345	0·489	0·639	0·747
0·65	0·091	0·211	0·348	0·497	0·656	0·754
0·70	0·094	0·217	0·357	0·507	0·661	0·749
0·75	0·101	0·225	0·356	0·499	0·637	0·727
0·80	0·100	0·216	0·348	0·484	0·620	0·704
0·85	0·093	0·204	0·323	0·446	0·552	0·632
0·90	0·090	0·184	0·274	0·364	0·459	0·535
0·95	0·066	0·123	0·185	0·247	0·309	0·375

TABLE 3

Variation with Chordwise Station of the Measured and Calculated Values of the Slope of the Normal-Force Characteristic at Zero Incidence.

$\dfrac{x}{c}$	$\left(\dfrac{dC_N(x)}{d\alpha}\right)_0$	$\dfrac{\bar{C}_{N_l}}{\alpha}$	$a(x)$	$\dfrac{\pi}{2}a(x)$
0			0·895	1·406
0·1	2·17	1·325		
0·2	2·25	1·362	0·918	1·442
0·3	2·30	1·385		
0·4	2·28	1·405	0·945	1·485
0·5	2·22	1·400		
0·6	2·12	1·381	0·967	1·520
0·7	1·95	1·350		
0·8	1·70	1·300	0·985	1·548
0·9	1·20	1·216		
1·0	0	1·062	1	1·571

TABLE 4

Variation with Incidence and Chordwise Station of the Non-Linear Normal-Force Component Induced by the Leading-Edge Vortices.

$\dfrac{x}{c}$	$\left(\dfrac{\partial C_N(x)}{\partial \alpha}\right)_0$	$\alpha = 8°$			$\alpha = 16°$		
		$\dfrac{C_N(x)}{\alpha}$	$\dfrac{\bar{C}_{N_{nl}}}{\alpha}$	$\dfrac{\bar{C}_{N_{nl}}}{\alpha}$	$\dfrac{C_N(x)}{\alpha}$	$\dfrac{\bar{C}_{N_{nl}}}{\alpha}$	$\dfrac{\bar{C}_{N_{nl}}}{\alpha}$
0·1	2·17	2·98	0·81	0·52	3·88	1·71	1·05
0·2	2·25	3·05	0·80	0·51	3·86	1·61	1·04
0·3	2·30	2·98	0·68	0·49	3·68	1·38	0·98
0·4	2·28	2·94	0·66	0·46	3·50	1·22	0·91
0·5	2·22	2·72	0·50	0·43	3·24	1·02	0·83
0·6	2·12	2·51	0·39	0·39	2·92	0·80	0·72
0·7	1·95	2·22	0·27	0·35	2·60	0·65	0·65
0·8	1·70	1·94	0·24	0·31	2·16	0·46	0·58
0·9	1·20	1·43	0·23	0·27	1·45	0·25	0·51
1·0	0	0	0	0·23	0	0	0·43

TABLE 5

Chordwise Variation of the Local Loading Coefficient on Five Delta Wings.

$\dfrac{\alpha}{K}$	A	$\dfrac{t}{c}$	Reference number	α, degree	$\dfrac{x}{c}$	$\dfrac{s}{b/2}C_N(x)$	$\dfrac{s}{b/2}\dfrac{C_N(x)}{K^2}$
0·712	1·616	0·048		16·5	0·1	0·115	0·70
					0·2	0·222	1·36
					0·3	0·315	1·93
					0·4	0·404	2·48
					0·5	0·465	2·85
					0·6	0·504	3·09
					0·7	0·525	3·22
					0·8	0·500	3·06
					0·9	0·378	2·32
					0·95	0·257	1·58
0·712	1·00	0·12	10	10·2	0·1	0·027	0·43
					0·2	0·058	0·93
					0·3	0·093	1·49
					0·4	0·130	2·08
					0·5	0·170	2·72
					0·6	0·209	3·34
					0·7	0·245	3·92
					0·8	0·254	4·06
					0·9	0·204	3·26
					0·95	0·137	2·19
0·712	1·00	0·05	16	10·2	0·26	0·099	1·57
					0·5	0·200	3·20
					0·75	0·248	3·96
0·712	1·00	0·021	17	10·2	0·3	0·141	2·25
					0·5	0·220	3·52
					0·7	0·245	3·92
					0·9	0·189	3·02
0·712	1·456	0·031	18	14·9	0·333	0·309	2·33
					0·5	0·398	3·0
					0·666	0·433	3·27
					0·833	0·387	2·92

TABLE 6

*Chordwise Variation of the Local Normal-Force Coefficient
on a Mild Gothic Wing and a Delta Wing.*

$\frac{x}{c}$	Delta, $A = 1.616$				Mild gothic, $A = 1.36$			
	α	$C_N(x)$	α	$C_N(x)$	α	$C_N(x)$	α	$C_N(x)$
0.10	8	0.425	16	1.110	8		16	
0.15		0.425		1.110				
0.20		0.425		1.075				
0.25		0.425		1.045		0.444		1.040
0.30		0.420		1.025		0.415		1.020
0.35		0.410		0.995		0.390		1.032
0.40		0.405		0.975		0.420		1.012
0.45		0.390		0.940		0.415		0.971
0.50		0.375		0.905		0.391		0.940
0.55		0.370		0.865		0.409		0.897
0.60		0.350		0.815		0.408		0.850
0.65		0.325		0.765		0.346		0.778
0.70		0.310		0.725		0.321		0.701
0.75		0.300		0.665		0.278		0.642
0.80		0.270		0.600		0.248		0.555
0.85		0.240		0.525		0.204		0.458
0.90		0.205		0.410		0.160		0.350
0.95		0.130		0.260		0.083		0.223

TABLE 7

*Longitudinal Characteristics of a Delta Wing
and a Mild Gothic Wing.*

α, deg	Delta, $A = 1.616$			Mild gothic, $A = 1.36$		
	C_L	C_D	C_M	C_L	C_D	C_M
2.5	0.080	0.010	-0.0024	0.080	0.011	-0.0005
5.0	0.178	0.025	-0.0048	0.175	0.022	-0.0018
7.5	0.282	0.044	-0.0073	0.270	0.040	-0.0030
10.0	0.393	0.072	-0.0084	0.375	0.068	-0.0037
12.5	0.506	0.115	-0.0085	0.480	0.104	-0.0034
15.0	0.620	0.170	-0.0084	0.592	0.154	-0.0019
17.5	0.738	0.235	-0.0080	0.710	0.217	0
20.0	0.860	0.315	-0.0062	0.827	0.292	0.0012
22.5	0.980	0.409	-0.0038	0.947	0.375	0.0045
25.0	1.106	0.514	$+0.0012$			

¢ chord = 50 in
Span   = 40·4 in
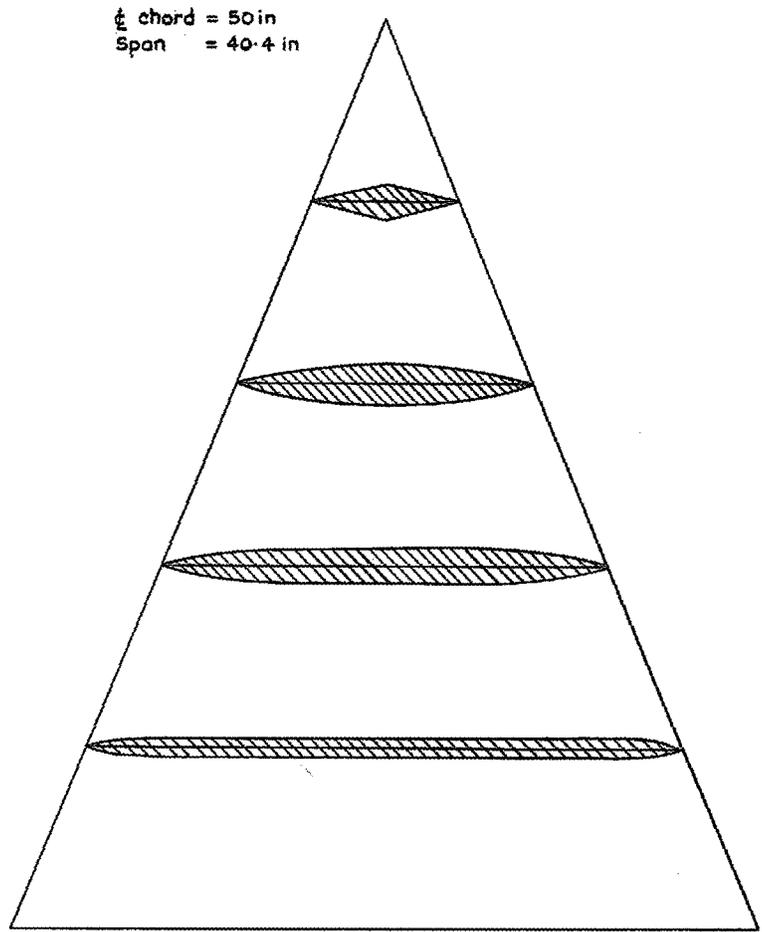
FIG. 1.   Planform and some typical cross-sections
of the wing tested.

0·05
0·10
0·15
0·20
0·25
0·30
0·35
0·40
0·45
0·50
0·55
0·60
0·65
0·70
0·75
0·80
0·85
0·90
x/c = 0·95

Cleat

y/s = 0·95 0·85 0·75 0·65
0·90 0·80 0·70 0·60 0·50 0·40 0·30 0·20 0·10

Sting bar
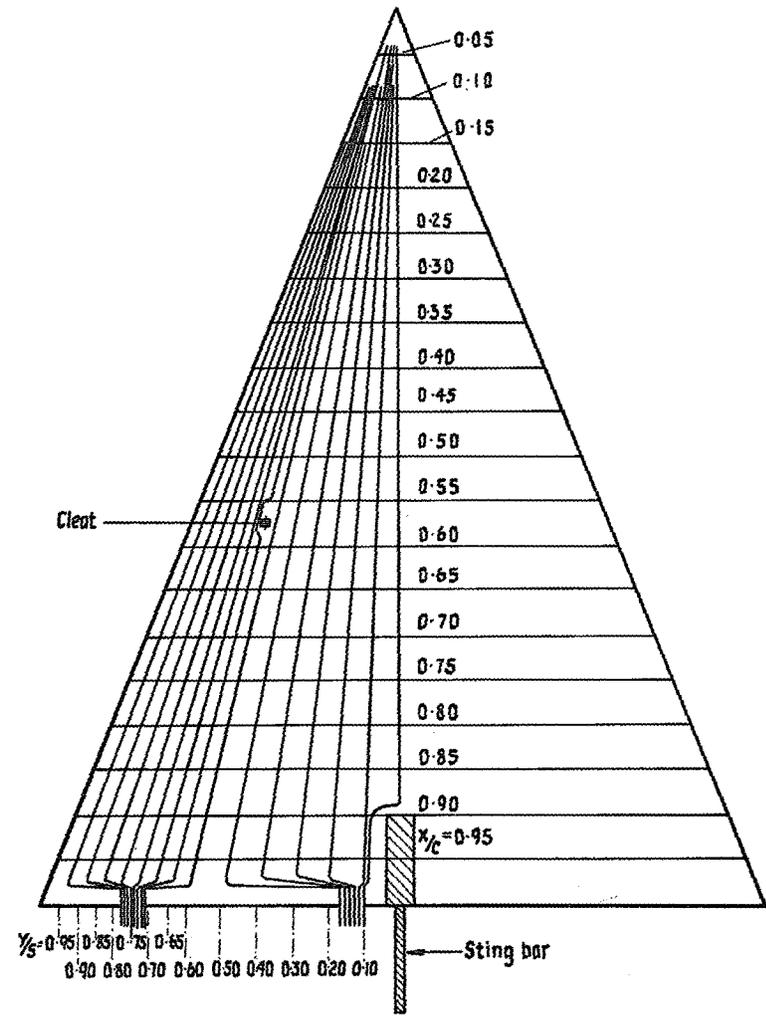
FIG. 2.   Plan view of the wing tested, showing the
position of the pressure tubing and the cleat on the
port side.
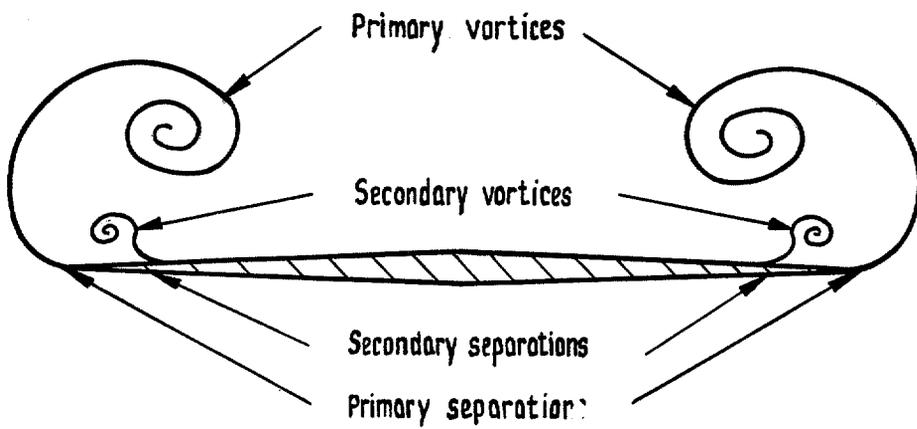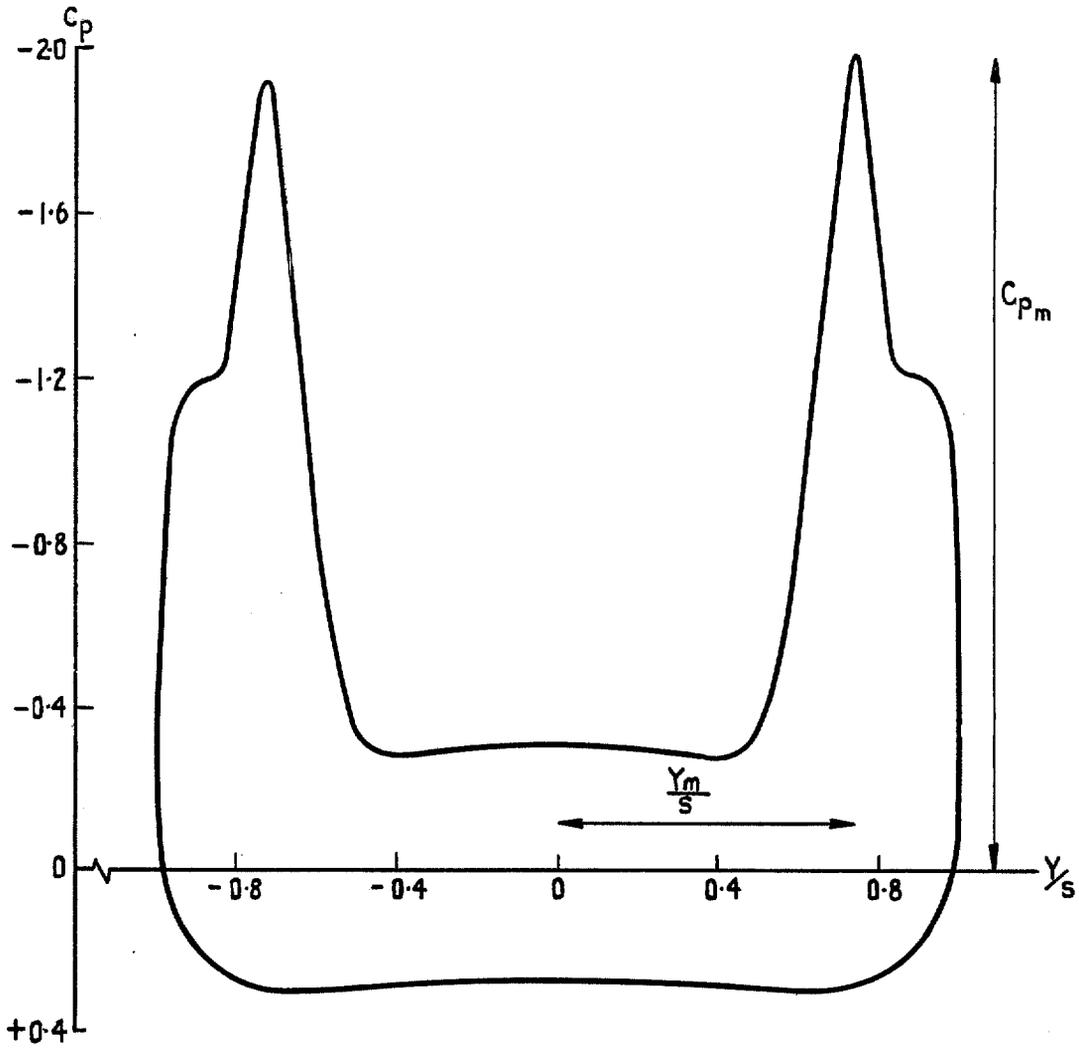
FIG. 3. Typical spanwise pressure distribution, and schematic spanwise cross-section of the associated flow field.
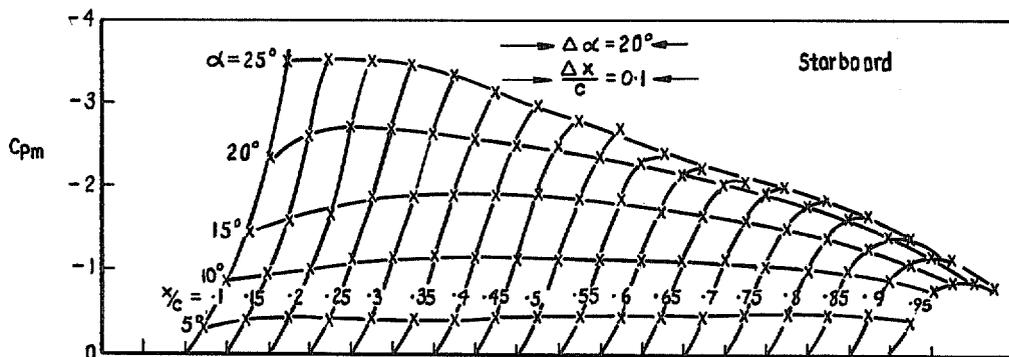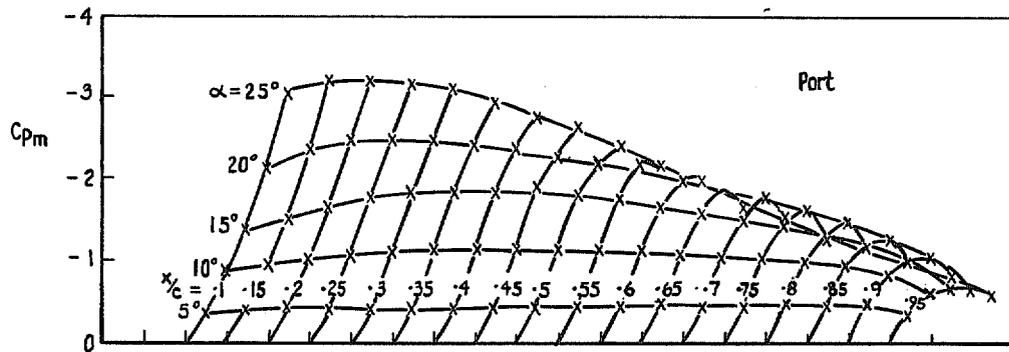
FIG. 4. Variation with incidence and chordwise station of the minimum static pressure.
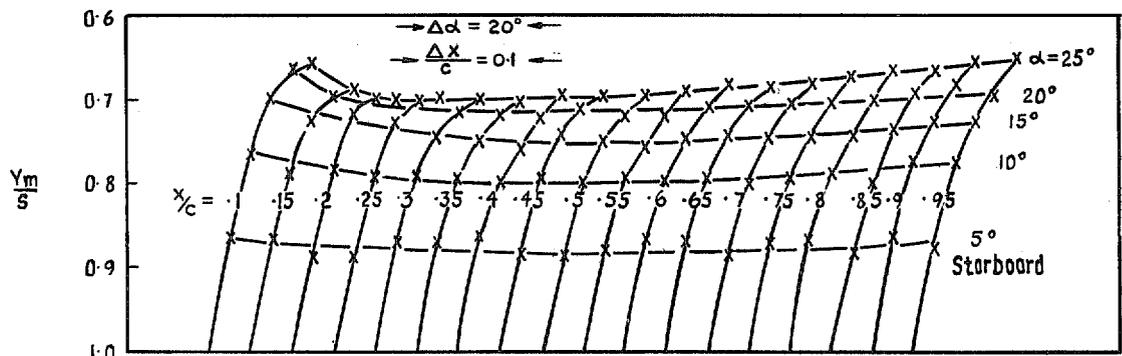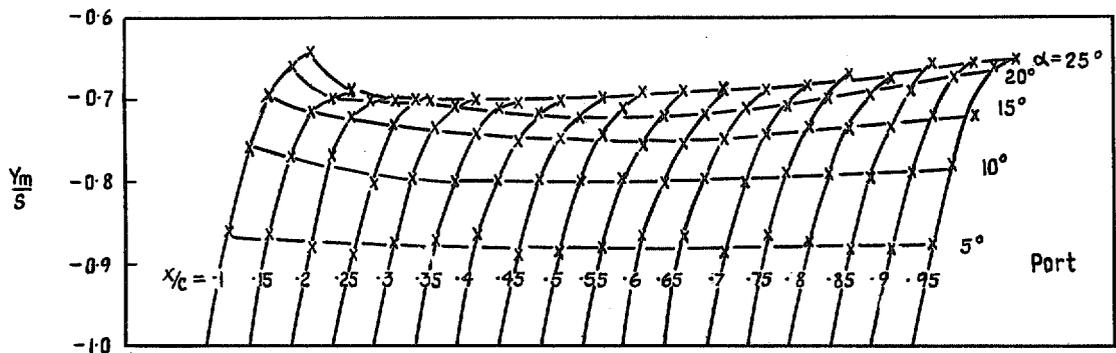
FIG. 5. Variation with incidence and chordwise station of the spanwise position of the minimum static pressure.
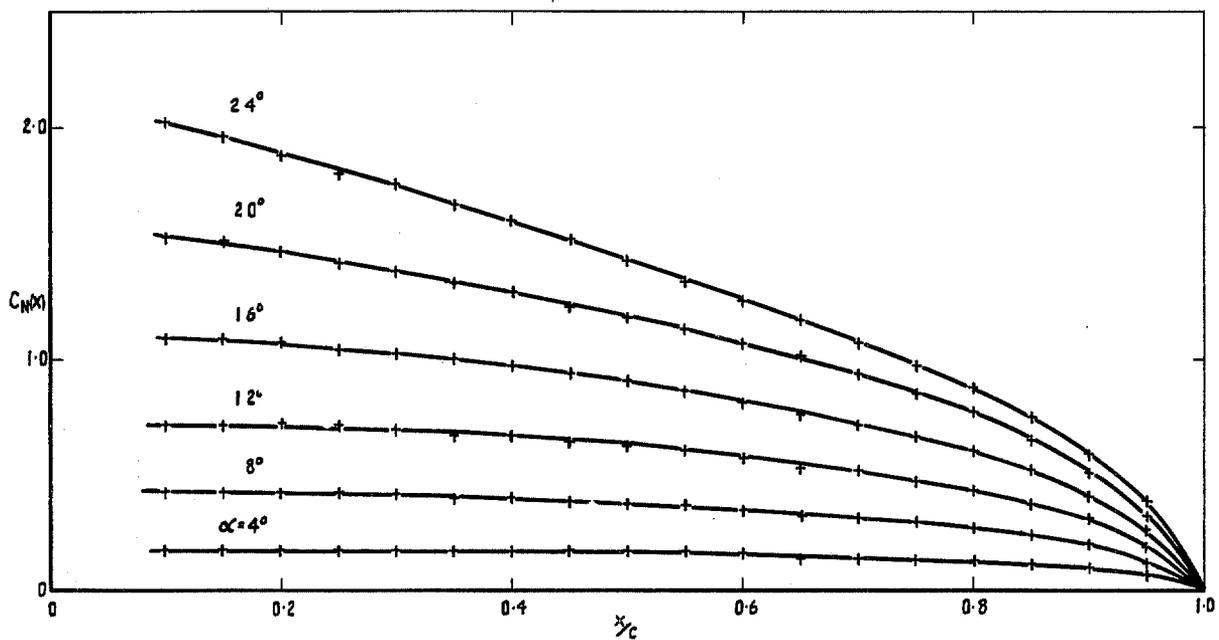
FIG. 6. Chordwise variation of the local normal-force coefficient.
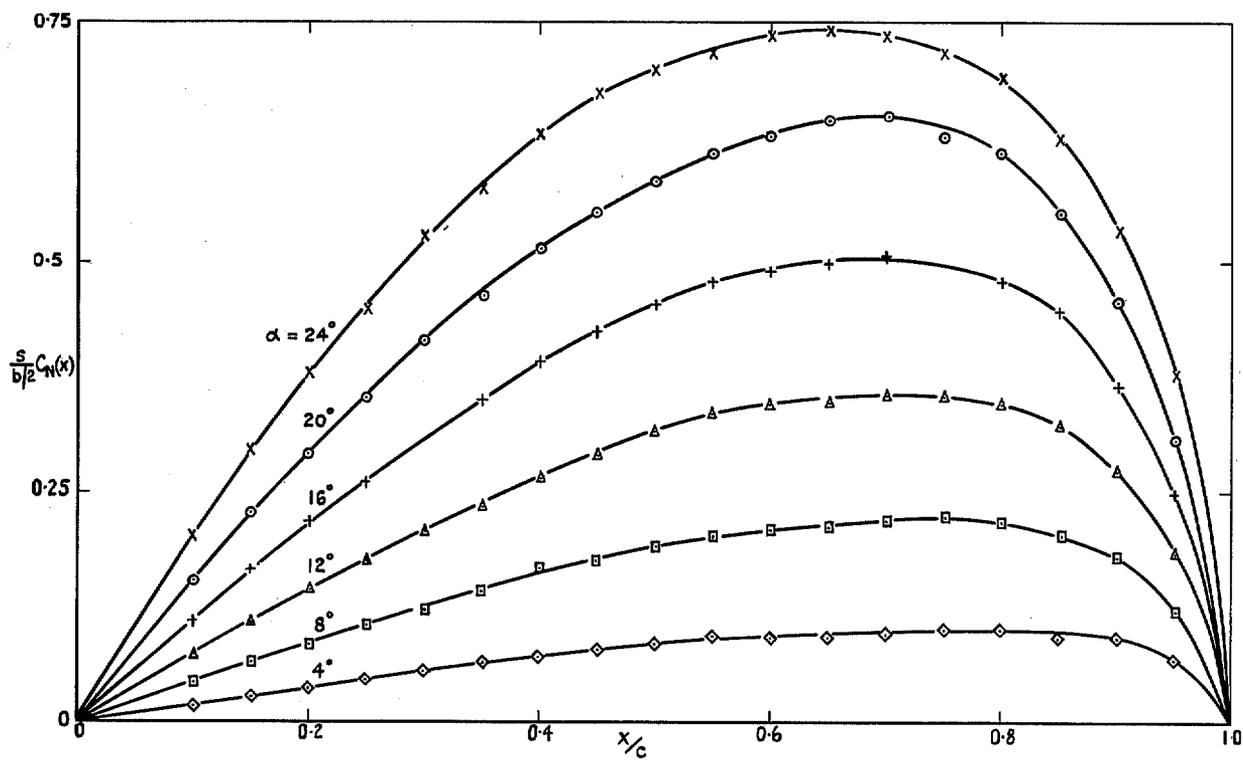
FIG. 7. Chordwise distribution of the aerodynamic loading.

23
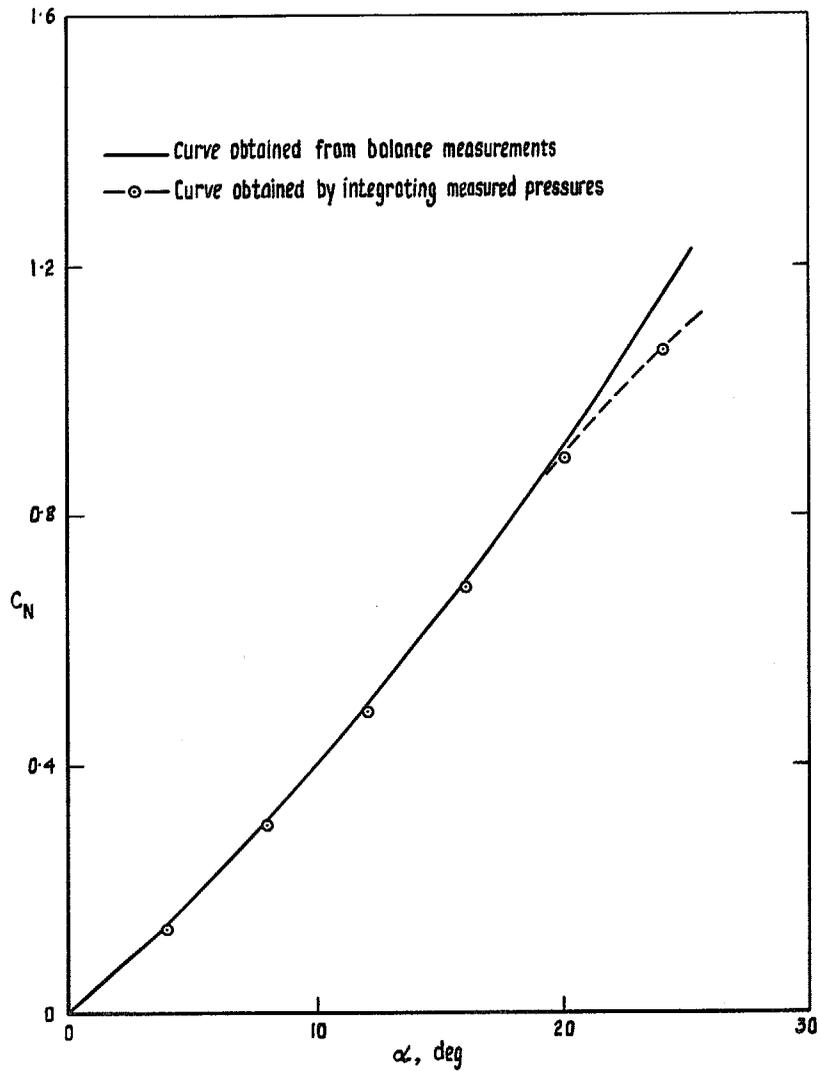
FIG. 8. Comparison of the normal-force characteristics obtained from pressure and balance measurements.
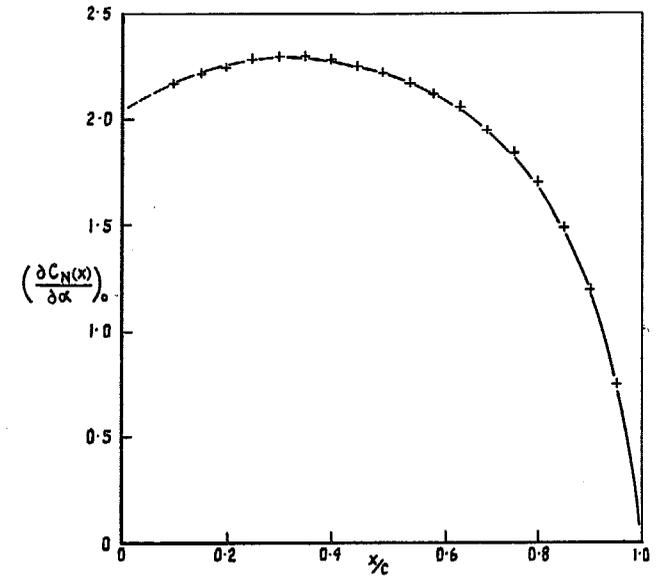
FIG. 9a. Chordwise variation of $\left(\dfrac{\partial C_N(x)}{\partial \alpha}\right)_0$.

FIG. 9b. Chordwise variation of $\dfrac{\overline{C}_{N_l}}{\alpha}$.

Incidence	Symbol
0°	+
8°	x
16°	⊙

Non-linear

linear
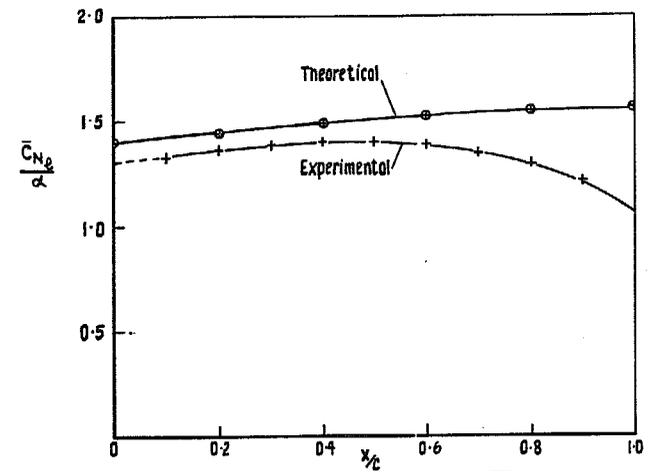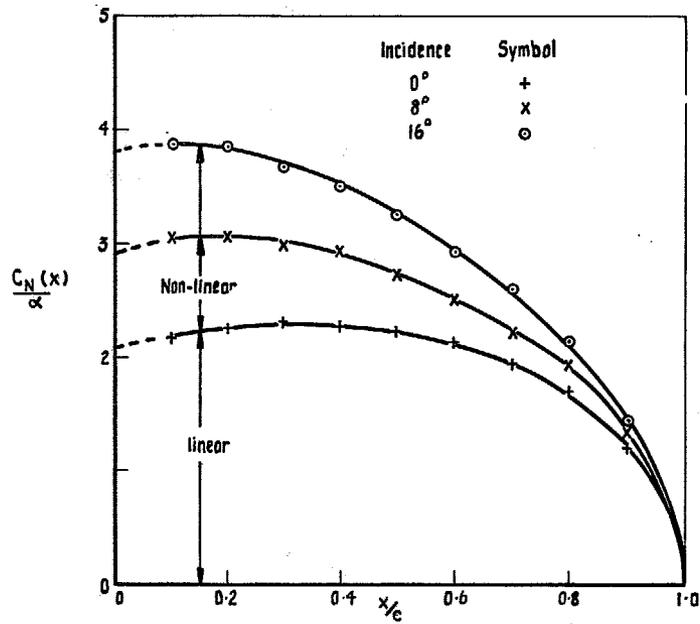
FIG. 10a. Chordwise variation of $\dfrac{C_N(x)}{\alpha}$.

Incidence	Symbol
8°	x
16°	⊙
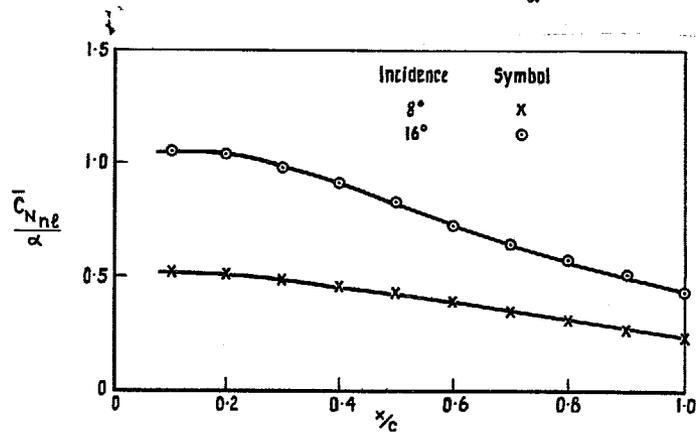
FIG. 10b. Chordwise variation of $\dfrac{\bar{C}_{N_{nl}}}{\alpha}$.

Plane delta wing in conical flow (ref 2)

$\dfrac{s}{b/2} \dfrac{C_N(x)}{K^2}$

$\dfrac{\alpha}{K} = 0.712$

Symbol	A	Max $t/2s$
⊙	1.0	0.047
x	1.456	0.043
+	1.616	0.31
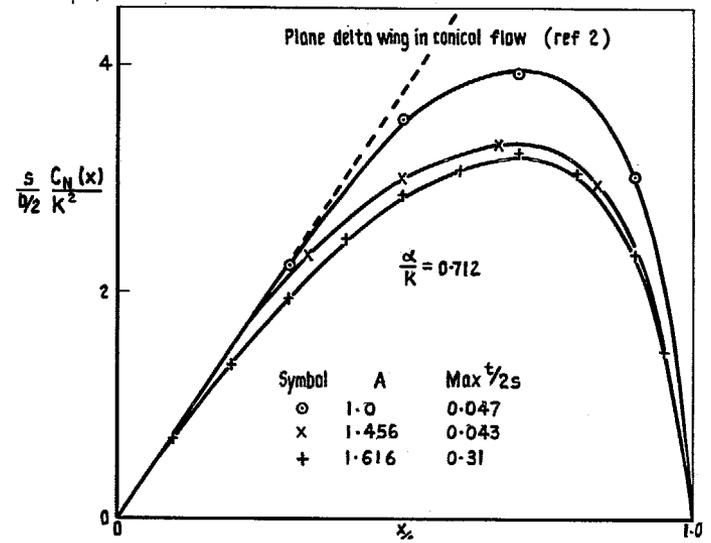
FIG. 11a. Chordwise loading distributions on thin delta wings.

Plane delta wing in conical flow (ref 2)

$\dfrac{s}{b/2} \dfrac{C_N(x)}{K^2}$

$\dfrac{\alpha}{K} = 0.712$

Symbol	A	Max $t/2s$
⊙	1.0	0.047
⊡	1.0	0.4
△	1.0	0.96
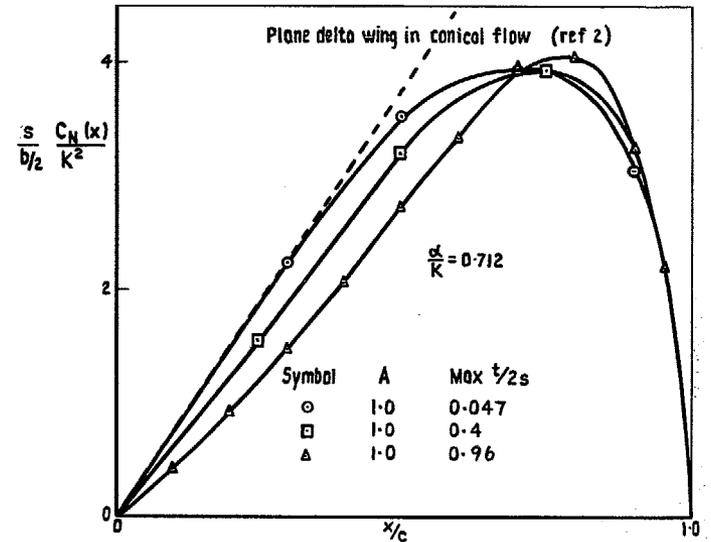
FIG. 11b. Chordwise loading distributions on delta wings of different thicknesses.
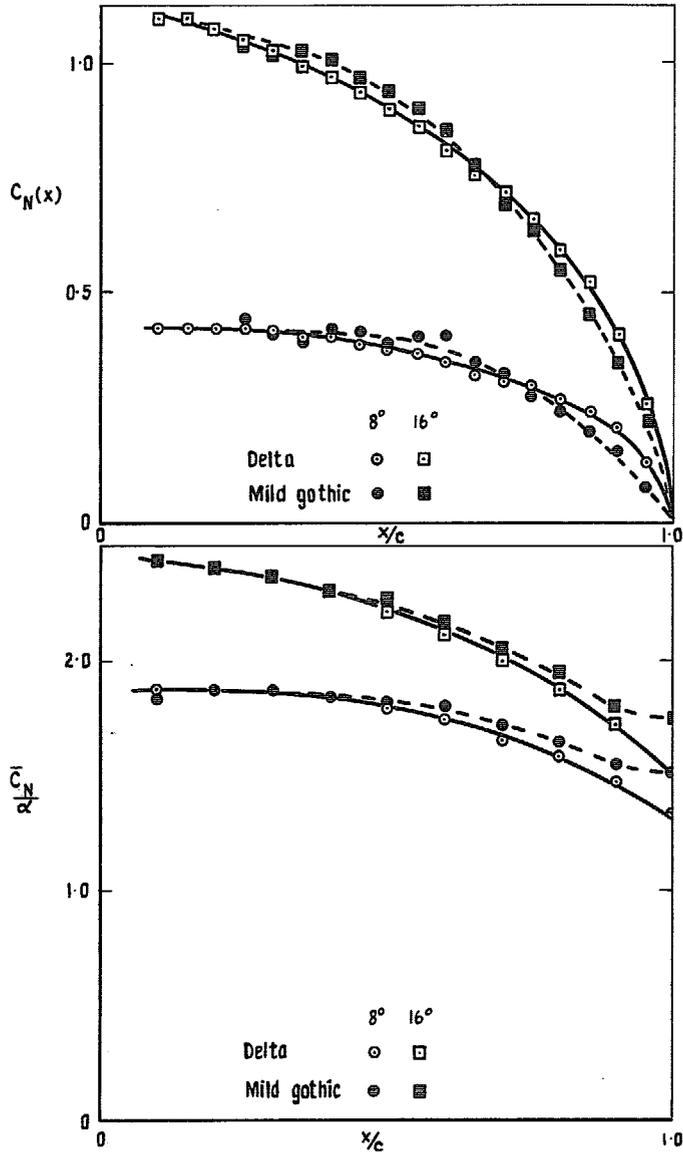
FIG. 12. Comparison of the aerodynamic loading
on a delta and on a mild gothic wing.
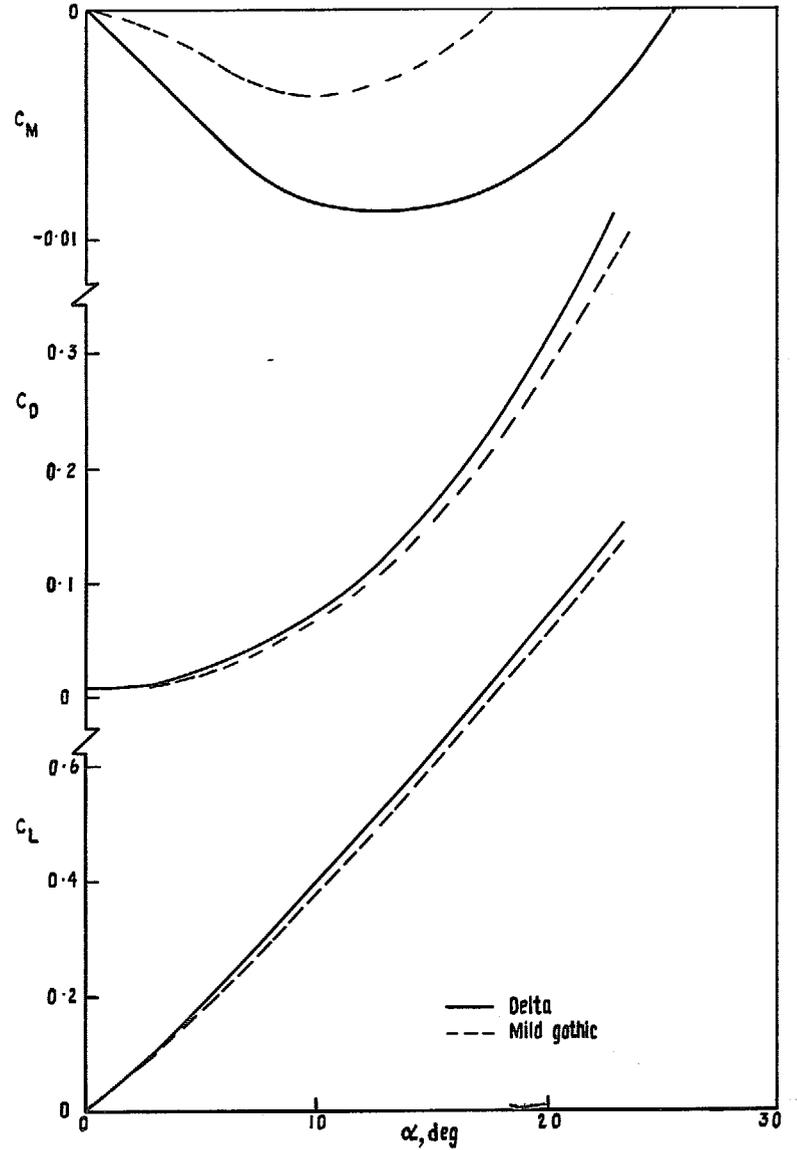
FIG. 13. Longitudinal characteristics of a delta
wing and a mild gothic wing.
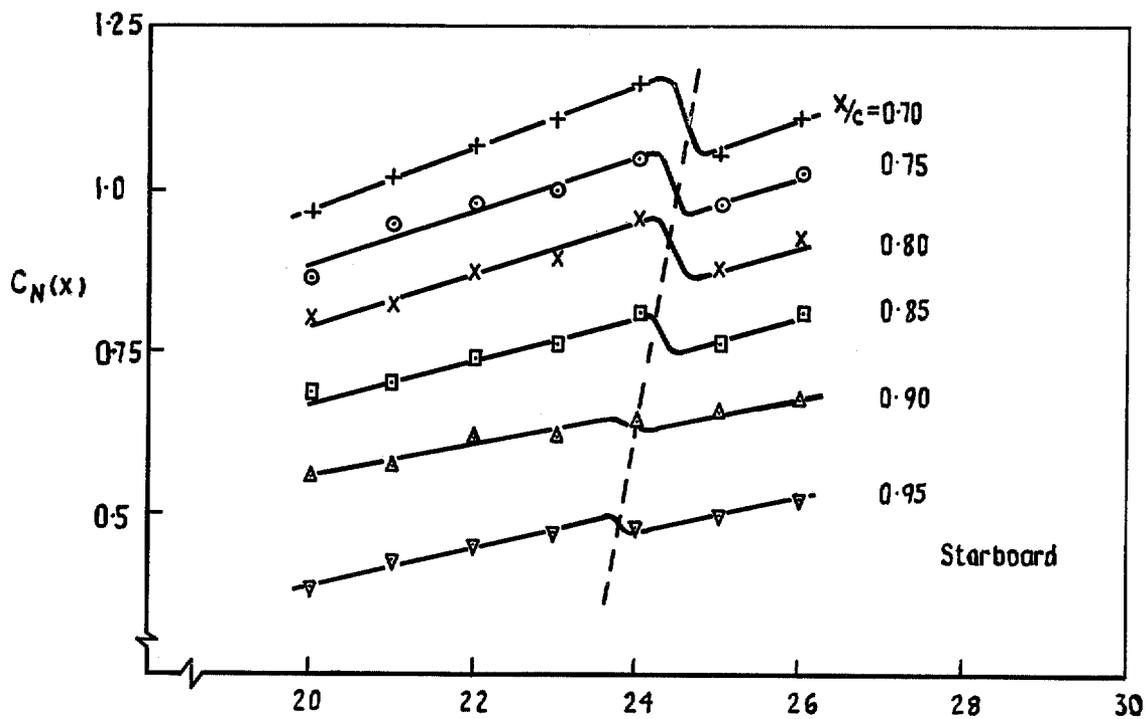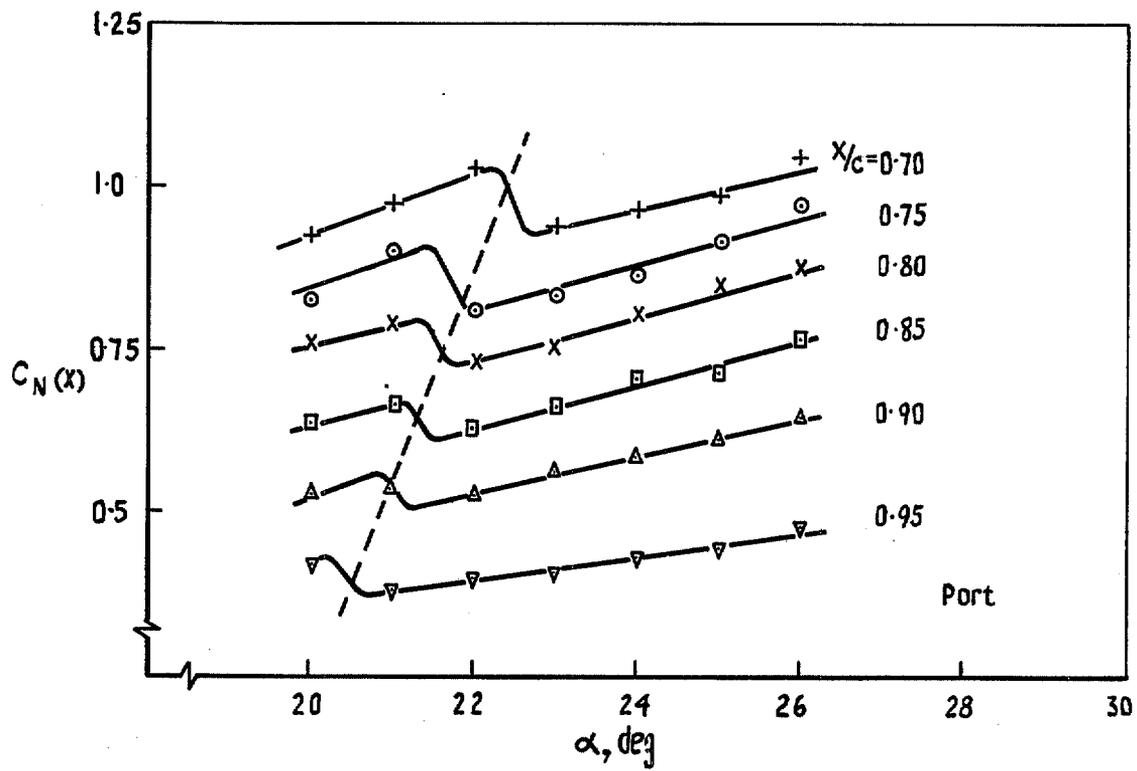
FIG. 14. Effect of vortex breakdown on local normal-force coefficients.